Comparisons of Proportional and Active-force Controls on Vibration of a Flexible Link Manipulator Using a Piezoelectric Actuator through Calculations and Experiments

Abdul Kadir Muhammad, Shingo Okamoto, Jae Hoon Lee, *Members, IAENG*

***Abstract*— The purposes of this research are to formulate the equations of motion of the system, to develop computational codes by a finite-element method in order to perform dynamics simulation with vibration control, to propose an effective control scheme using two control strategies, namely proportional (P) and active-force (AF) controls and to confirm the calculated results by experiments of a flexible link manipulator. The system used in this paper consists of an aluminum beam as a flexible link, a clamp-part, a servo motor to rotate the link and a piezoelectric actuator to control vibration. Computational codes on time history responses, FFT (Fast Fourier Transform) processing and eigenvalues - eigenvectors analysis were developed to calculate the dynamic behavior of the link. Furthermore, the P and AF controls strategies were designed and compared their performances through calculations and experiments. The calculated and experimental results showed the superiority of the proposed AF control compared to the P one to suppress the vibration of the flexible link manipulator.**

***Index Terms*—Active-force control, Finite-element method, flexible manipulator, piezoelectric actuator, vibration control.**

I. Introduction

EMPLOYMENT of flexible link manipulator is recommended in the space and industrial applications in order to accomplish high performance requirements such as high-speed besides safe operation, increasing of positioning accuracy and lower energy consumption, namely less weight. However, it is not usually easy to control a flexible manipulator because of its inheriting flexibility. Deformation of the flexible manipulator when it is operated must be considered by any control. Its controller system should be dealt with not only its motion but also vibration due to the flexibility of the link.

In the past few decades, a number of modeling methods and control strategies using piezoelectric actuators to deal with the vibration problem have been investigated by researchers [1] – [7]. Nishidome and Kajiwara [1] investigated a way to enhance performances of motion and vibration of a flexible-link mechanism. They used a modeling method based on modal analysis using the finite-element method. The model was described as a state space form. Their control system was constructed with a designed dynamic compensator based on the mixed of H_2/H_∞. They recommended separating the motion and vibration controls of the system. Yavus Yaman et al [2] and Kircali et al [3] studied an active vibration control technique on aluminum beam modeled in cantilevered configuration. The studies used the ANSYS package program for modeling. They investigated the effect of element selection in finite-element modeling. The model was reduced to state space form suitable for application of H_∞ [2] and spatial H_∞ [3] controllers to suppress vibration of the beam. They showed the effectiveness of their techniques through simulation. Zhang et al [4] has studied a flexible piezoelectric cantilever beam. The model of the beam using finite-elements was built by ANSYS application. Based on the Linear Quadratic Gauss (LQG) control method, they introduced a procedure to suppress the vibration of the beam with the piezoelectric sensors and actuators were symmetrically collocated on both sides of the beam. Their simulation results showed the effectiveness of the method. Gurses et al [5] investigated vibration control of a flexible single-link manipulator using three piezoelectric actuators. The dynamic modeling of the link had been presented using Euler-Bernoulli beam theory. Composite linear and angular velocity feedback controls were introduced to suppress the vibration. Their simulation and experimental results showed the effectiveness of the controllers. Xu and Koko [6] studied finite-element analysis and designed controller for flexible structures using piezoelectric material as actuators and sensors. They used a commercial finite-element code for modeling and completed with an optimal active vibration control in state space form. The effectiveness of the control method was confirmed through simulations. Kusculuoglu et al [7] had used a piezoelectric actuator for excitation and control vibrations of a beam. The beam and actuator were modeled using Timoshenko beam theory. An optimized vibration absorber using an electrical resistive-inductive shun circuit on the actuator was used as a passive controller. The effectiveness of results was shown by simulations and experiment.

Furthermore, applications of the AF control strategy to suppress vibration of a flexible system were done by some researchers [8] – [10]. Hewit et al [8] used the AF control for deformation and disturbance attenuation of a flexible manipulator. Then, a PD control was used for trajectory tracking of the flexible manipulator. They used a motor as an actuator. Modeling of the manipulator was done using virtual link coordinate system (VLCS). Their simulation results had shown that the proposed control could cancel the disturbance

Manuscript received June 26, 2014

Every author is with Mechanical Engineering Course, Graduate School of Science and Engineering, Ehime University, 3 Bunkyo-cho, Matsuyama 790-8577, Japan. (e-mail: y861008b@mails.cc.ehime-u.ac.jp, kadir_muhammad@yahoo.co.id, okamoto.shingo.mh@ehime-u.ac.jp, jhlee@ehime-u.ac.jp).

The first author is also with Center for Mechatronics and Control System, Mechanical Engineering Department, State Polytechnic of Ujung Pandang, Jl. Perintis Kemerdekaan KM 10 Makassar, 90-245, Indonesia.

satisfactorily. Tavakolvour et al [9] investigated the AF control application for a flexible thin plate. Modeling of their system was done using finite-difference method. Their calculated results showed the effectiveness of the proposed controller to reduce vibration of the plate. Tavakolvour and Mailah [10] studied the AF control application for a flexible beam with an electromagnetic actuator. Modeling of the beam was done using finite-difference method. The effectiveness of the proposed controller was confirmed through simulation and experiment.

The purposes of this research are to derive the equations of motion of a flexible single-link system by a finite-element method, to develop the computational codes in order to perform dynamics simulations with vibration control, to propose an effective control scheme of a flexible single-link manipulator using two control strategies, namely proportional (P) and active-force (AF) controls and to confirm the calculated results by experiments of the flexible link manipulator.

The flexible manipulator used in this paper consists of an aluminum beam as a flexible link, a clamp-part, a servo motor to rotate the link and a piezoelectric actuator to control vibration. Computational codes on time history responses, FFT (Fast Fourier Transform) processing and eigenvalues - eigenvectors analysis were developed to calculate the dynamic behavior of the link and validated by the experimental one. Furthermore, the P and AF controls strategies were designed to suppress the vibration. It was done by adding bending moments generated by the piezoelectric actuator to the single-link. Finally, their performances were compared through calculations and experiments.

II. Formulation by Finite-element Method

The link has been discretized by finite-elements [11] - [12]. The finite-element has two degrees of freedom, namely the lateral deformation $v(t)$, and the rotational angle $\psi(t)$. The length, the cross-sectional area and the area moment of inertia around z-axis of every element are denoted by l_i, S_i and I_{zi} respectively. Mechanical properties of every element are denoted as Young's modulus E_i and mass density ρ_i.

A. Kinematic

Figure 1 shows the position vector of an arbitrary point P in the link in the global and rotating coordinate frames. Let the link as a flexible beam has a motion that is confined in the horizontal plane as shown in figure 1. The $O - XY$ frame is the global coordinate frame while $O - xy$ is the rotating coordinate frame fixed to the root of the link. A motor is installed on the root of the link. The rotational angle of the motor when the link rotates is denoted by $\theta(t)$.

The position vector $\boldsymbol{r}(x,t)$ of the arbitrary point P in the link at time $t = t$, measured in the $O - XY$ frame shown in figure 1 is expressed by

$$\boldsymbol{r}(x,t) = X(x,t)\boldsymbol{I} + Y(x,t)\boldsymbol{J} \tag{1}$$

Where

$$X(x,t) = x\cos\theta(t) - v(x,t)\sin\theta(t) \tag{2}$$

$$Y(x,t) = x\sin\theta(t) + v(x,t)\cos\theta(t) \tag{3}$$

The velocity of P is given by

$$\dot{\boldsymbol{r}}(x,t) = \dot{X}(x,t)\boldsymbol{I} + \dot{Y}(x,t)\boldsymbol{J} \tag{4}$$

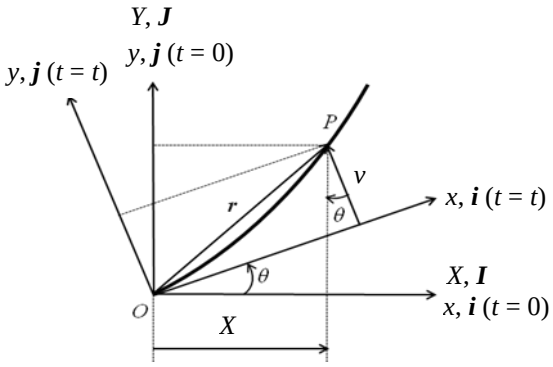

$O - XY$: Global coordinate frame
$O - xy$: Rotating coordinate frame

Fig. 1. Position vector of an arbitrary point P in the link in the global and rotating coordinate frames

B. Finite-element Method

Figure 2 shows the rotating coordinate frame and the link divided by one-dimensional and two-node elements. Then, figure 3 shows the element coordinate frame of the *i-th* element. Here, there are four boundary conditions together at nodes i and (i+1) when the one-dimensional and two-node element is used. The four boundary conditions are expressed as nodal vector as follow

$$\boldsymbol{\delta}_i = \{v_i \quad \psi_i \quad v_{i+1} \quad \psi_{i+1}\}^T \tag{5}$$

Then, the hypothesized deformation has four constants as follows [13]

$$v_i = a_1 + a_2 x_i + a_3 {x_i}^2 + a_4 {x_i}^3 \tag{6}$$

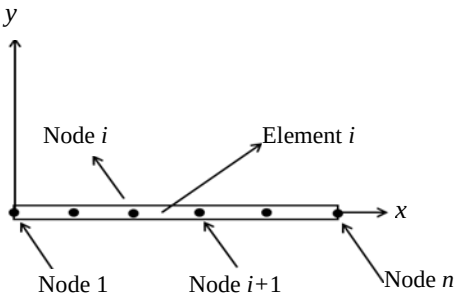

$o - xy$: Rotating coordinate frame

Fig. 2. Rotating coordinate frame and the link divided by the one-dimensional and two-node elements

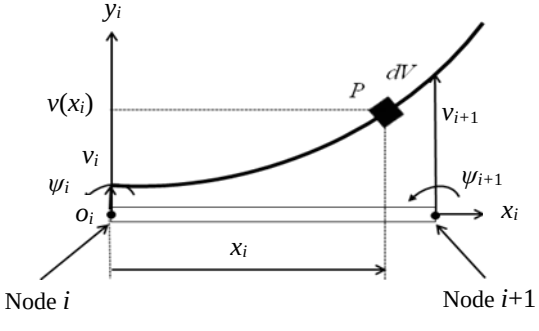

$o_i - x_i\, y_i$: Element coordinate frame of the i-th element

Fig. 3. Element coordinate frame of the *i-th* element

The relation between the lateral deformation v_i and the rotational angle ψ_i of the node i is given by

$$\psi_i = \frac{\partial v_i}{\partial x_i} \tag{7}$$

Furthermore, from mechanics of materials, the strain of node i can be defined by

$$\varepsilon_i = \varepsilon_{x_i} = -y_i \frac{\partial^2 v_i}{\partial {x_i}^2} \tag{8}$$

C. Equations of motion

Equation of motion of the *i-th* element is given by

$$\boldsymbol{M}_i \ddot{\boldsymbol{\delta}}_i + \boldsymbol{C}_i \dot{\boldsymbol{\delta}}_i + \left[\boldsymbol{K}_i - \dot{\theta}^2(t)\boldsymbol{M}_i\right]\boldsymbol{\delta}_i = \ddot{\theta}(t)\,\boldsymbol{f}_i \tag{9}$$

where $\boldsymbol{M}_i$, $\boldsymbol{C}_i$, $\boldsymbol{K}_i$, $\ddot{\theta}(t)\,\boldsymbol{f}_i$ are the mass matrix, damping matrix, stiffness matrix and the excitation force generated by the rotation of the motor respectively. The representation of the matrices and vector in Eq. (9) can be found in [11]. Finally, the equation of motion of the system with n elements considering the boundary conditions is given by

$$\boldsymbol{M}_n \ddot{\boldsymbol{\delta}}_n + \boldsymbol{C}_n \dot{\boldsymbol{\delta}}_n + \left[\boldsymbol{K}_n - \dot{\theta}^2(t)\boldsymbol{M}_n\ \boldsymbol{\delta}_n\right] = \ddot{\theta}(t)\,\boldsymbol{f}_n \tag{10}$$

III. Validation of Formulation and Computational Codes

A. Experimental Model

Figure 4 shows the experimental model of the flexible link manipulator. The flexible link manipulator consists of the flexible aluminum beam, the clamp-part, the servo motor and the base. The link is attached to the motor through the clamp-part. A strain gage is bonded to the position of 0.11 m from the origin of the link. The motor is mounted to the base. In the experiments, the motor was operated by an independent motion controller.

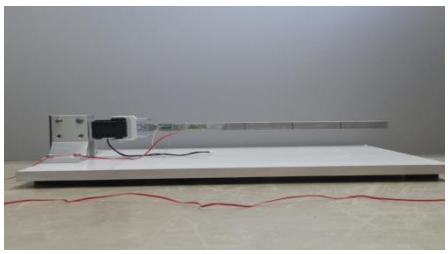

Fig. 4. Experimental model of the flexible link manipulator

B. Computational Model

In this research, we defined and used two types of computational models of the flexible link manipulator.

Model I

A model of only a flexible link manipulator was used as Model Ⅰ. Figure 5.a shows model Ⅰ. The link and the clamp-part were discretized by 5 elements and 1 element respectively. The clamp-part is much rigid than the link. Therefore Young's modulus of the clamp-part was set in 1,000 times of the link's. A strain gage is bonded to the position of Node 3 of the flexible link (0.11 m from the origin of the link).

Model II

A model of the flexible link manipulator including the piezoelectric actuator was defined as Model Ⅱ. Figure 5.b shows model Ⅱ. The piezoelectric actuator was bonded to the one surface of element 2. The link was discretized by 22 elements. A schematic representation on modeling of the piezoelectric actuator is shown in figure 6. Physical parameters of the flexible link manipulator model and the piezoelectric actuator are shown in table 1.

The piezoelectric actuator suppressed the vibration of the flexible link manipulator by adding bending moments at Nodes 2 and 3, M_2 and M_3 to the flexible link. The bending moments are generated by applying voltages $+E$ to the piezoelectric actuator as shown in figure 6. The relation between the bending moments and the voltages are related by

$$M_{2,3} = \pm d_1 E \tag{11}$$

Here d_1 is a constant quantity.

Furthermore, the voltage to generate the bending moments is proportional to the strain ε of the single-link due to the vibration. The relation can be expressed as follows

$$E = \pm \frac{1}{d_2}\varepsilon \tag{12}$$

Here d_2 is a constant quantity. Then, d_1 and d_2 will be determined by comparing the calculated results and experimental ones.

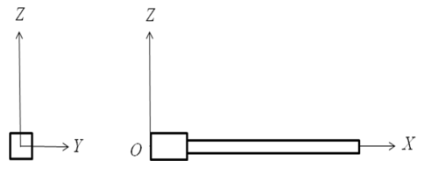

(a) Model Ⅰ: Only flexible link

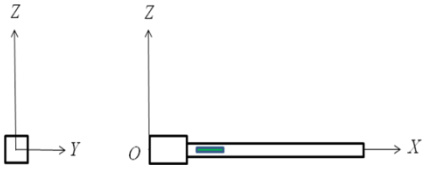

(b) Model Ⅱ: Flexible link with the actuator

Fig. 5. Computational models of the flexible link manipulator

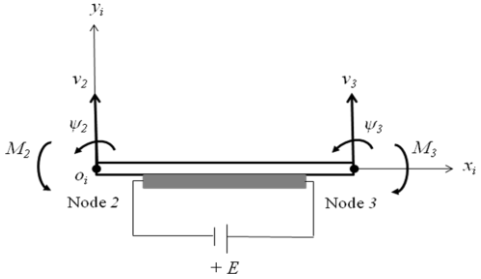

Fig. 6. Modeling of the piezoelectric actuator

TABLE I
PHYSICAL PARAMETERS OF THE FLEXIBLE LINK AND THE PIEZOELECTRIC ACTUATOR [14]

l : Total length	m	3.91×10^{-1}
l_l : Length of the link	m	3.50×10^{-1}
l_c : Length of the clamp-part	m	4.10×10^{-2}
l_a : Length of the actuator	m	2.00×10^{-2}
S_l : Cross section area of the link	m^2	1.95×10^{-5}
S_c : Cross section area of the clamp-part	m^2	8.09×10^{-4}
S_a : Cross section area of the actuator	m^2	1.58×10^{-5}
I_{zl} : Cross section area moment of inertia around z-axis of the link	m^4	2.75×10^{-12}
I_{zc} : Cross section area moment of inertia around z-axis of the clamp-part	m^4	3.06×10^{-8}
I_{za} : Cross section area moment of inertia around z-axis of the actuator	m^4	1.61×10^{-11}
E_l : Young's Modulus of the link	GPa	7.03×10^{1}
E_c : Young's Modulus of the clamp-part	GPa	7.00×10^{4}
E_a : Young's Modulus of the actuator	GPa	4.40×10^{1}
ρ_l : Density of the link	kg/m^3	2.68×10^{3}
ρ_c : Density of the clamp-part	kg/m^3	9.50×10^{2}
ρ_a : Density of the actuator	kg/m^3	3.33×10^{3}
α : Damping factor of the link	-	2.50×10^{-4}

C. Time History Responses of Free Vibration

Experiment on free vibration was conducted using an impulse force as an external one. Figure 7 shows the experimental time history response of strains ε_e on the free vibration at the same position in the calculation. Furthermore, the computational codes on time history response of Model I were developed. Figure 8 shows the calculated strains at Node 3 of Model I under the impulse force.

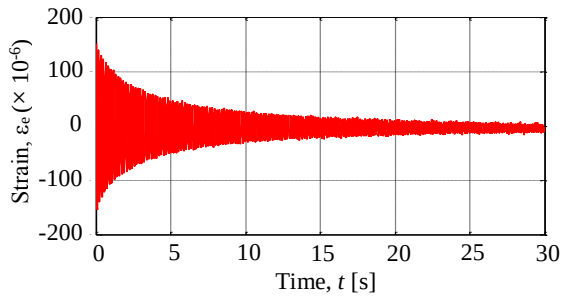

Fig. 7. Experimental time history response of strains on free vibration of the flexible link at 0.11 m from the origin of the link

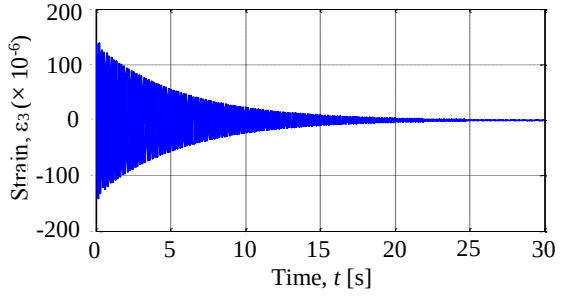

Fig. 8. Calculated time history response of strains on free vibration at Node 3 of Model I

D. Fast Fourier Transform (FFT) Processing

Both the experimental and calculated time history responses of free vibration of Model I were transferred by FFT processing to find their frequencies.

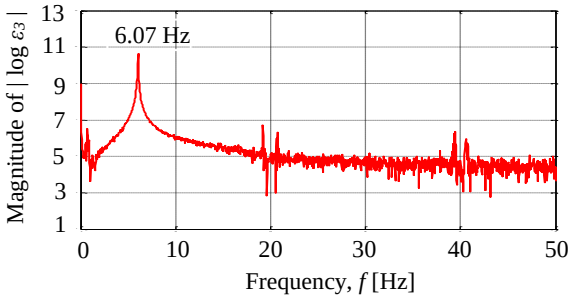

Fig. 9. Experimental natural frequencies of the flexible link

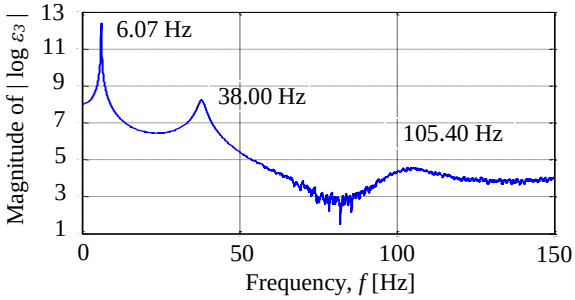

Fig. 10. Calculated natural frequencies of Model I

Figures 9 and 10 shows the experimental and calculated natural frequencies of the flexible link manipulator, respectively. The experimental first natural frequency, 6.07 Hz well agreed with the calculated one. The second and third experimental natural frequencies could not be measured. However, in the calculation, they could be obtained as 38.00 Hz and 105.40 Hz.

E. Eigen-values and Eigen-vectors Analysis

The computational codes on Eigen-values and Eigen-vectors analysis were developed for natural frequencies and vibration modes.

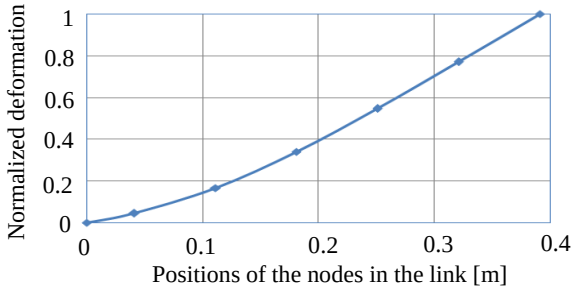

Fig. 11. First vibration mode and natural frequency ($f_1 = 6.10$ Hz) of Model I

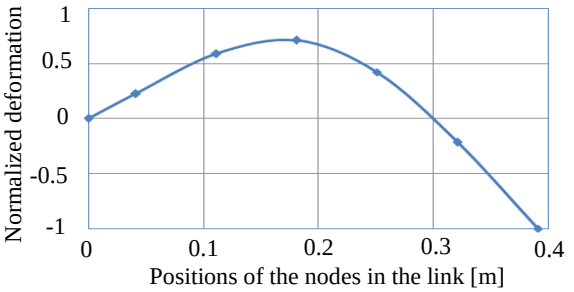

Fig. 12. Second vibration mode and natural frequency ($f_2 = 38.22$ Hz) of Model I

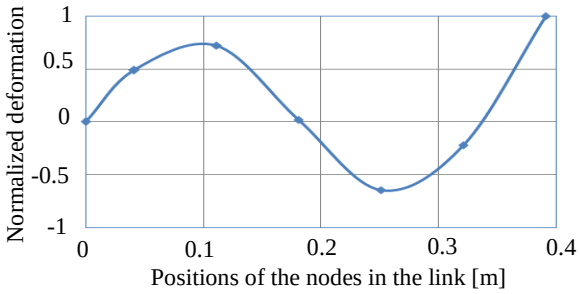

Fig. 13. Third vibration mode and natural frequency (f_3 = 107.19 Hz) of Model I

The calculated results for the first, second and third natural frequencies were 6.10 Hz, 38.22 Hz, and 107.19 Hz respectively. The vibration modes of natural frequencies are shown in figure 11, 12 and 13

F. Time History Responses due to Base Excitation

Another experiment was conducted to investigate the vibration of the flexible link due to the base excitation generated by rotation of the motor. In the experiment, the motor was rotated by the angle of $\pi/2$ radians (90 degrees) within 2.05 seconds. Figure 14 shows the experimental time history response of strains of the flexible link due to the motor's rotation at 0.11 m from the origin of the link. Based on figure 14, the angular acceleration of the motor was calculated. Time history response of the motor's acceleration is shown in figure 15. Furthermore, based on figures 14 and 15, the time history response of strains at Node 3 of Model I was calculated as shown in figure 16.

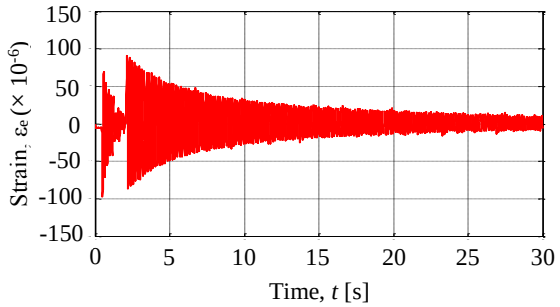

Fig. 14. Experimental time history responses of strains at 0.11 m from the origin of the link due to the base excitation

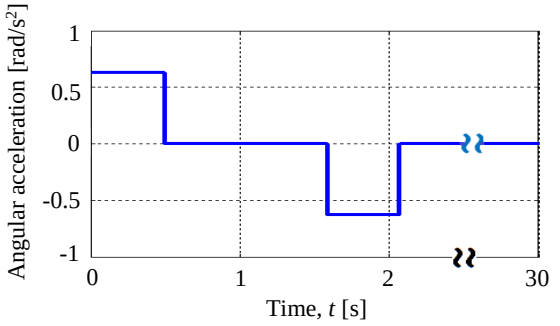

Fig. 15. Time history response of angular acceleration of the motor

The above results show the validities of the formulation, computational codes and modeling the flexible link manipulator.

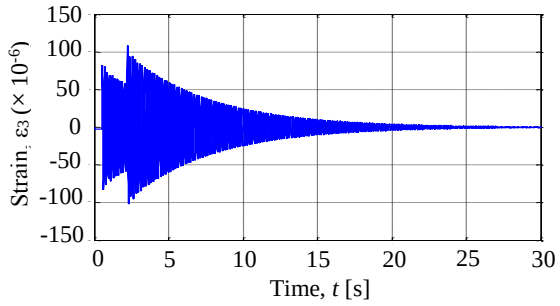

Fig. 16. Calculated time history responses of strains at Node 3 of Model I due to the base excitation

IV. Control Scheme

A control scheme to suppress the vibration of the single-link was designed using the piezoelectric actuator. It was done by adding bending moments generated by the piezoelectric actuator to the single-link. Therefore, the equation of motion of the system become

$$\boldsymbol{M}_n\ddot{\boldsymbol{\delta}}_n + \boldsymbol{C}_n\dot{\boldsymbol{\delta}}_n + \left[\boldsymbol{K}_n - \dot{\theta}^2(t)\boldsymbol{M}_n\right]\boldsymbol{\delta}_n = \ddot{\theta}(t)\,\boldsymbol{f}_n + \boldsymbol{u}_n(t) \quad (13)$$

where the vector of $\boldsymbol{u}_n(t)$ containing M_2 and M_3 is the control force generated by the actuator to the single-link.

To drive the actuator, two different control strategies namely P and AF controls have been designed and examined. Their performances were compared through calculations and experiments.

A. Proportional Control

Substituting Eq. (12) to Eq. (11) gives

$$M_{2,3} = \pm\frac{d_1}{d_2}\varepsilon \quad (14)$$

Based on Eq. (14), the bending moments can be defined in *s*-domain as follows

$$\boldsymbol{U}_n(s) = \boldsymbol{G}_C(s)\left(\varepsilon_d(s) - \varepsilon_3(s)\right) \quad (15)$$

where ε_d and ε_3 denote the desired and measured strains at Node 3, respectively. The gain of P-controller can be written by a vector in *s*-domain as follows

$$\boldsymbol{G}_C(s) = \left\{0 \quad 0 \quad 0 \quad K_p \quad 0 \quad -K_p \quad 0 \quad \cdots \quad 0\right\}^T \quad (16)$$

A block diagram of the proportional control strategy for the single-link system is shown in Fig. 17.

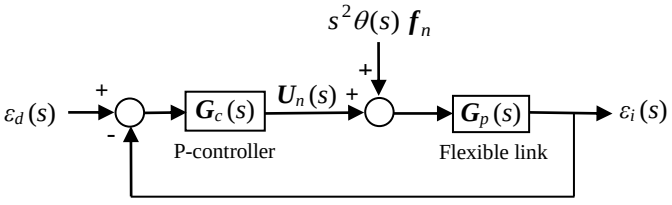

ε_d: Desired strain, ε_i: Measured strains at Node i
θ: Rotation angle of the motor, $\boldsymbol{U}_n$: Applied bending moments

Fig. 17. Block diagram of proportional control of the flexible link manipulator

B. Active-force Control

Fig. 18 shows the block diagram of the AF control that is proposed in this research. In this strategy, vibration of the system is controlled by canceling bending moments acting at Nodes 2 and 3 due to the base excitation (excitation bending moments). The following steps are the way to estimate and cancel the excitation bending moments.

Firstly, the strain, ε_3 at Node 3 is measured to estimate the lateral deformation, v_3 at the Node 3. Substituting Eq. (6) to Eq. (8) considering the boundary conditions then the relation between the strain and the lateral deformation can be defined as follows

$$\frac{v_3}{\varepsilon_3} = -\frac{x^2(x-3l)}{6y(x-l)} = A \tag{17}$$

where l, x and y are the length of the link, the position of Node 3 in x and y directions, respectively.

Secondly, the actual force in the s-domain acting at Node 3 can be defined in the form of the Newton's equation of motion as follows

$$F_3(s) = M_{33}\, s^2\, v_3 \tag{18}$$

where M_{33} is the component of the mass matrix corresponding to Node 3.

Thirdly, the bending moments acting at Nodes 2 and 3 are estimated using the following equation

$$\boldsymbol{U}_{nt}(s) = \pm F_3(s)\,\boldsymbol{d} \tag{19}$$

The vector $\boldsymbol{d}$ that represents the position vector from the reference point to the position where the excitation force acting can be written as follows

$$\boldsymbol{d} = \{0 \quad 0 \quad 0 \quad l_2 \quad 0 \quad l_2 \quad 0 \quad \cdots \quad 0\}^T \tag{20}$$

Fourthly, based on Fig. 18, the excitation bending moments can be calculated as

$$\boldsymbol{U}_{ne}(s) = K_{pa}\left\{\boldsymbol{U}_{nt}(s) - \boldsymbol{U}_n(s)\right\} \tag{21}$$

where K_{pa} is the non-dimensional proportional gain of the proposed AF control.

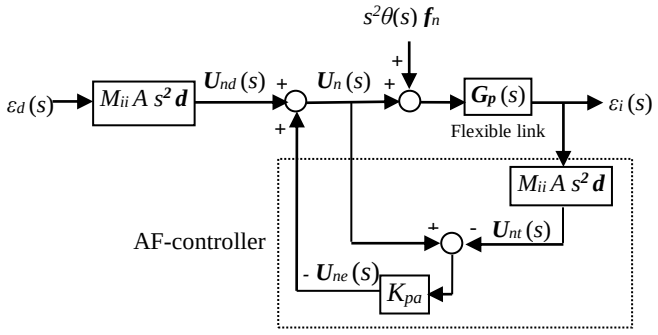

ε_d : Desired strain, ε_i : Measured strains at Node i
θ : Rotation angle of the motor, M_{ii} : Component of mass matrix
A : Conversion from ε_i to v_i, $\boldsymbol{d}$: Position vector
$\boldsymbol{U}_{nd}$: Desired bending moments, $\boldsymbol{U}_n$: Applied bending moments
$\boldsymbol{U}_{ne}$: Excitation bending moments, $\boldsymbol{U}_{nt}$: Bending moments

Fig. 18. Block diagram of active-force control of the flexible link manipulator

Finally, the bending moments applying as a control force to control the vibration of the system can be calculated as follows

$$\boldsymbol{U}_n(s) = -\boldsymbol{U}_{ne}(s) + \boldsymbol{U}_{nd}(s) \tag{22}$$

where $\boldsymbol{U}_{nd}(s)$ is the desired bending moments which is zero. The negative of $\boldsymbol{U}_{ne}(s)$ indicates that the bending moments used to cancel the vibration of the system.

V. Experiment

A. Experimental Set-up

In order to investigate the validity of the proposed control strategies, an experimental set-up was designed. The set-up is shown in Fig.19. The flexible link manipulator consists of the flexible aluminum beam, the clamp-part, the servo motor and the base. The flexible link was attached to the motor through the clamp-part. In the experiments, the motor was operated by an independent motion controller. A strain gage was bonded to the position of 0.11 m from the origin of the link.

The piezoelectric actuator was attached on one side of the flexible manipulator to provide the blocking force against vibrations. A Wheatstone bridge circuit was developed to measure the changes in resistance of the strain gage in the form of voltages. An amplifier circuit was designed to amplify the small output signal of the Wheatstone bridge.

Furthermore, a data acquisition board and a computer that have functionality of A/D (analog to digital) conversion, signal processing, control process and D/A (digital to analog) conversion were used. The data acquisition board connected to the computer through USB port. Finally, the controlled signals sent to a piezo driver to drive the piezoelectric actuator in its voltage range.

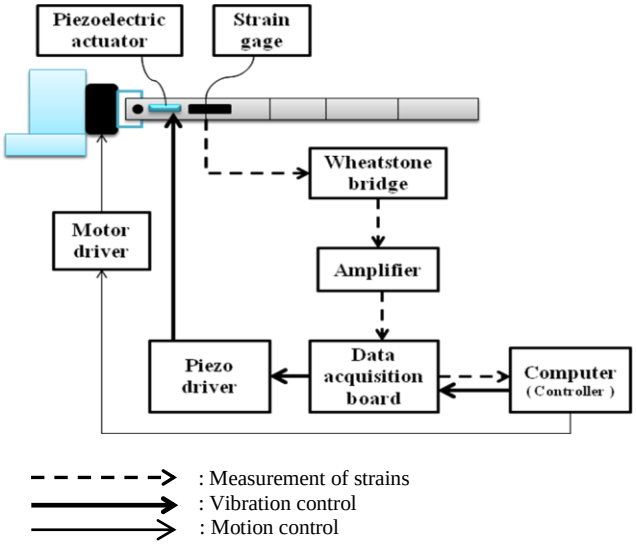

Fig. 19. Schematics of measurement and control system [12]

B. Experimental Method

The rotation of the motor was set from 0 to $\pi/2$ radians (90 degrees) within 0.68 second. The outputs of strain gage were converted to voltages by the Wheatstone bridge and magnified by the amplifier. The noises that occur in the experiment were reduced by a 100 μF capacitor attached to the amplifier. The output voltages of the amplifier sent to the data acquisition board and the computer for control process.

Both of control strategies were implemented in the computer using the visual C++ program. The analog output voltages of the data acquisition board sent to the input channel of the piezo driver to generate the actuated signals for the piezoelectric actuator.

VI. Calculated and Experimental Results

A. Calculated Results

Time history responses of strains on the uncontrolled and controlled systems were calculated when the motor rotated by the angle of $\pi/2$ radians (90 degrees) within 0.68 seconds. Time history responses of strains on the controlled system were calculated for Model II under two control strategies as shown in figures 17 and 18.

Examining several gains of the P and AF controllers leaded to K_p = 600 [Nm] and K_{pa} = 0.83[-] as the better ones. Figure 19 shows the uncontrolled and controlled time history responses of strains at Node 3. The maximum and minimum strains of uncontrolled system in positive and negative sides were 348.00×10^{-6} and -452.50×10^{-6}, as shown in figure 19(a). By using P-controller they became 167.50×10^{-6} and -131.00×10^{-6}, as shown in figure 19(b). Moreover, by using AF-controller they became 86.50×10^{-6} and -69.00×10^{-6}, as shown in figure 19(c).

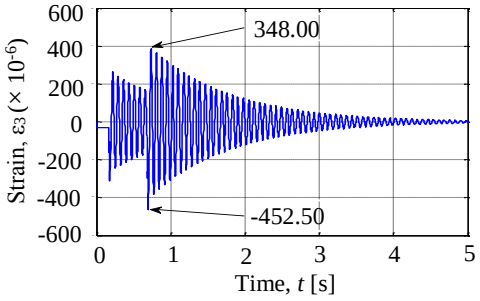

(a) Uncontrolled system

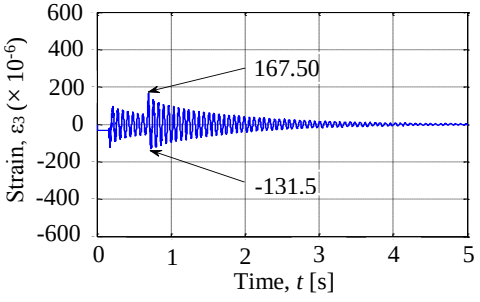

(b) Controlled by P-controller, K_p = 600 [Nm]

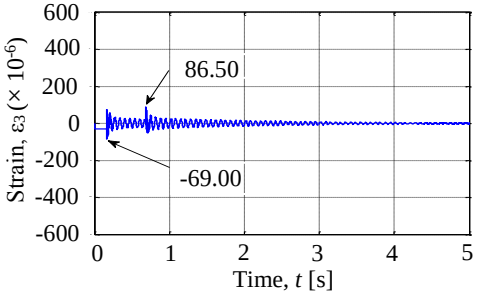

(c) Controlled by AF-controller, K_{pa} = 0.83 [-]

Fig. 19. Calculated time history response of strains at Node 3 for uncontrolled and controlled Model II due to the base excitation

B. Experimental Results

Experimental time history responses of the strains on the uncontrolled and controlled systems were measured when the motor rotated by the angle of $\pi/2$ radians (90 degrees) within 0.68 seconds. Experimental time history responses on the controlled system were measured under two control strategies as shown in figures 17 and 18.

Based on the calculated results, the experimental proportional gains that are non-dimensional gain, K_p' were examined. The examination of gains leaded to K_p' = 600 [-] as the better one. Furthermore, examining several gains of the active-force control leaded to K_{pa} = 125 [-] as the better one. Figure 20 shows the experimental uncontrolled and controlled time history responses of strains at the same position in the calculations. The maximum and minimum strains of uncontrolled system in positive and negative sides were 359.40×10^{-6} and -440.40×10^{-6}, as shown in figure 20(a). By using P-controller they became 262.40×10^{-6} and -373.40×10^{-6}, as shown in figure 20(b). Moreover, by using AF-controller they became 175.50×10^{-6} and -303.50×10^{-6}, as shown in figure 20(c).

It was verified from these results that the vibration of the flexible link manipulator can be more effectively suppressed using the proposed active-force control compared to the proportional one.

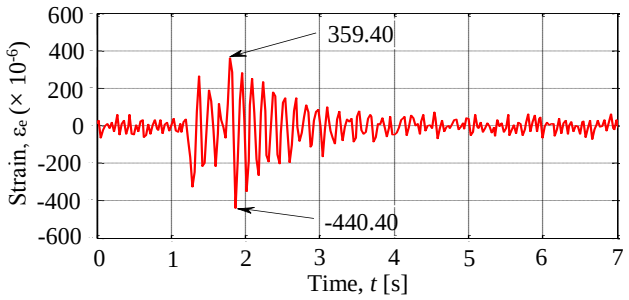

(a) Uncontrolled system

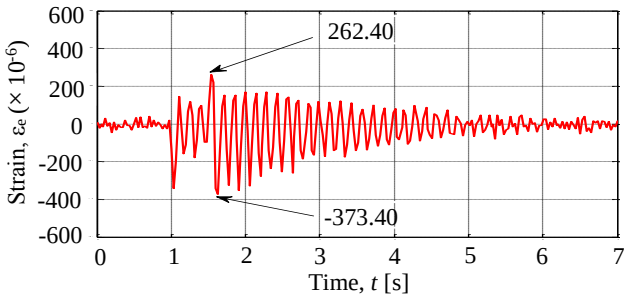

(b) Controlled by P-controller, K_p' = 600 [-]

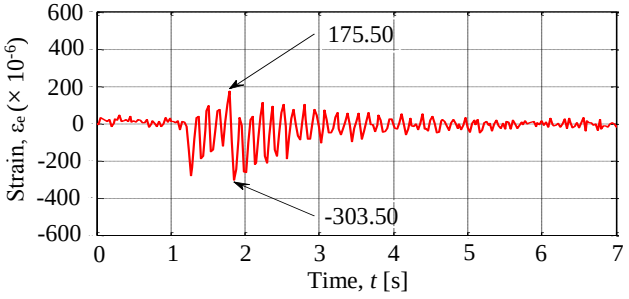

(c) Controlled by AF-controller, K_{pa} = 125 [-]

Fig. 20. Experimental time history responses of strains at 0.11 m from the link's origin for uncontrolled and controlled system due to the base excitation

VII. Conclusion

The equations of motion for the flexible link manipulator had been derived using the finite-element method. Computational codes had been developed in order to perform dynamic simulations of the system. Experimental and calculated results on time history responses, natural frequencies and vibration modes show the validities of the formulation, computational codes and modeling of the system. The proportional (P) and active-force (AF) controls strategies were designed to suppress the vibration of the system. Their performances were compared through the calculations and experiments. The calculated and experimental results show the superiority of the proposed active-force control comparing the proportional one to suppress the vibration of the flexible single-link manipulator.

References

[1] C. Nishidome, and I. Kajiwara, "Motion and Vibration Control of Flexible-link Mechanism with Smart Structure", *JSME International Journal*, vol.46, no.2, 2003, pp. 565 – 571.

[2] Y. Yaman et al, "Active Vibration Control of a Smart Beam", *Proceedings of the 2001 CANSMART Symposium*, 2001, pp. 125 – 134.

[3] O.F. Kircali et al, "Active Vibration Control of a Smart Beam by Using a Spatial Approach", *New Developments in Robotics, Automation and Control*, 2009, pp. 378 – 410.

[4] J. Zhang et al, "Active Vibration Control of Piezoelectric Intelligent Structures", *Journal of Computers*, Vol. 5. No. 3, 2010, pp. 401 – 409.

[5] K. Gurses et al, Vibration control of a single-link flexible manipulator using an array of fiber optic curvature sensors and PZT actuators, *Mechatronics* 19, 2009, pp. 167 – 177.

[6] S.X. Xu and T.S. Koko, "Finite Element Analysis and Design of Actively Controlled Piezoelectric Smart Structures", *Finite Elements in Analysis and Design* 40, 2004, pp. 241 – 262.

[7] Z.K. Kusculuoglu et al, "Finite Element Model of a Beam with a Piezoceramic Patch Actuator", *Journal of Sound and Vibration* 276, 2004, pp. 27 – 44.

[8] J.R. Hewit et al, "Active Force Control of a Flexible Manipulator by Distal Feedback", *Mech. Mach. Theory* Vol. 32, No. 5, 1997, pp. 583 – 596.

[9] A.R. Tavakolpour et al, "Modeling and Simulation of a Novel Active Vibration Control System for a Flexible Structures", *WSEAS Transaction on System and Control* Issue 5, Vol. 6, 2011, pp. 184 – 195.

[10] A.R. Tavakolpour and M. Mailah, "Control of Resonance Phenomenon in Flexible Structures Via Active Support", *Journal of Sound and Vibration* 331, 2012, pp. 3451 – 3465.

[11] A.K. Muhammad et al, "Computer Simulations on Vibration Control of a Flexible Single-link Manipulator Using Finite-element Method", *Proceeding of 19th International Symposium of Artificial Life and Robotics*, 2014, pp. 381 – 386.

[12] A.K. Muhammad et al, "Computer Simulations and Experiments on Vibration Control of a Flexible Link Manipulator Using a Piezoelectric Actuator", *Lecture Notes in Engineering and Computer Science: Proceeding of The International MultiConference of Engineers and Computer Scientists* 2014, IMECS 2014, 12 – 14 March, 2014, Hong Kong, pp. 262 – 267.

[13] M. Lalanne et al, *Mechanical Vibration for Engineers*, John Wiley & Sons Ltd, 1983, pp. 146 – 153.

[14] www.mmech.com, *Resin Coated Multilayer Piezoelectric Actuators.*